Tracer-based metabolomics for profiling nitric oxide metabolites in a 3D microvessels-on-chip model

Kallakkudi Pandian, K.; Huang, L.; Junaid, A.O.; Harms, A.C.; Zonneveld, A.J. van; Hankemeier, T.

Note: To cite this publication please use the final published version (if applicable).

The FASEB Journal

RESEARCH ARTICLE

Tracer-based metabolomics for profiling nitric oxide metabolites in a 3D microvessels-on-chip model

Kanchana Pandian[1] | Luojiao Huang[1] | Abidemi Junaid[1] | Amy Harms[1] |
Anton Jan van Zonneveld[2] | Thomas Hankemeier[1]

[1]Division of Systems Biomedicine and Pharmacology, LACDR, Leiden University, Leiden, the Netherlands

[2]Department of Internal Medicine (Nephrology) and the Einthoven Laboratory for Vascular and Regenerative Medicine, Leiden University Medical Center (LUMC), Leiden, the Netherlands

Correspondence
Anton Jan van Zonneveld, Department of Internal Medicine (Nephrology) and the Einthoven Laboratory for Vascular and Regenerative Medicine, Leiden University Medical Center (LUMC), Leiden, the Netherlands.
Email: a.j.van_zonneveld@lumc.nl

Present address
Abidemi Junaid, Wyss Institute for Biologically Inspired Engineering, Harvard University, Boston, Massachusetts, USA

Abstract

Endothelial dysfunction, prevalent in cardiovascular diseases (CVDs) and linked to conditions like diabetes, hypertension, obesity, renal failure, or hypercholesterolemia, is characterized by diminished nitric oxide (NO) bioavailability—a key signaling molecule for vascular homeostasis. Current two-dimensional (2D) in vitro studies on NO synthesis by endothelial cells (ECs) lack the crucial laminar shear stress, a vital factor in modulating the NO-generating enzyme, endothelial nitric oxide synthase (eNOS), under physiological conditions. Here we developed a tracer-based metabolomics approach to measure NO-specific metabolites with mass spectrometry (MS) and show the impact of fluid flow on metabolic parameters associated with NO synthesis using 2D and 3D platforms. Specifically, we tracked the conversion of stable-isotope labeled NO substrate L-Arginine to L-Citrulline and L-Ornithine to determine eNOS activity. We demonstrated clear responses in human coronary artery endothelial cells (HCAECs) cultured with $^{13}C_6$, $^{15}N_4$-L-Arginine, and treated with eNOS stimulator, eNOS inhibitor, and arginase inhibitor. Analysis of downstream metabolites, $^{13}C_6$, $^{15}N_3$ L-Citrulline and $^{13}C_5$, $^{15}N_2$ L-Ornithine, revealed distinct outcomes. Additionally, we evaluated the NO metabolic status in static 2D culture and 3D microvessel models with bidirectional and unidirectional fluid flow. Our 3D model exhibited significant effects, particularly in microvessels exposed to the eNOS stimulator, as indicated by the $^{13}C_6$, $^{15}N_3$ L-Citrulline/$^{13}C_5$, $^{15}N_2$ L-Ornithine ratio, compared to the 2D culture. The obtained results indicate that the 2D static culture mimics an endothelial dysfunction status, while the 3D model with a unidirectional fluid flow provides a more representative physiological environment that provides a better model to study endothelial dysfunction.

KEYWORDS
3D microvessel model, endothelial dysfunction, eNOS, nitric oxide metabolites, shear stress

1 | INTRODUCTION

Nitric oxide is an essential diatomic molecule generated by eNOS/NOS3 and that exerts multiple key roles in vascular homeostasis, including vasodilation and inflammation. The eNOS enzyme can be activated by multiple physiological (oxygen and shear stress)[1] or humoral (bradykinin and insulin) cues that drive diverse phosphorylation events on multiple sites such as serine 114, 615, 633, 1177, 1179, and threonine 495 in the oxygenase and reductase domains of the protein.[2] When released from the endothelium, NO diffuses into vascular stromal cells such as pericytes or smooth muscle cells to promote vascular relaxation through the stimulation of cyclic guanosine monophosphate (cGMP) synthesis by soluble guanylyl cyclase.[3–5]

Dysregulation of NO signaling pathways is associated with pathophysiological conditions such as endothelial dysfunction, a main driver for atherogenesis and cardiometabolic disorders.[6–8] In endothelial dysfunction, reduced availability of NO converts the endothelial cell phenotype to a pro-inflammatory state with increased oxidative stress and a loss of vasodilatory capacity.[9,10] At the molecular level, multiple factors have been reported to contribute to the loss of NO generation in endothelial dysfunction, including a deficiency in the substrate L-arginine or co-factors such as flow-mediated dilation (FMD), nicotinamide adenine dinucleotide phosphate (NADPH), or tetrahydrobiopterin (BH_4). For instance, when BH_4 is converted to BH_2 (7,8-dihydrobiopterin) in an oxidative environment, the eNOS enzyme gets uncoupled from the cofactor leading to the generation of superoxide rather than NO.[11–16]

At the physiological level, it is well established that fluid shear stress enhances the activity of eNOS.[17,18] Endothelial cells detect changes in local hemodynamics through mechanosensors located on the luminal side of the membrane, within focal adhesions on the abluminal side, and within cell–cell junctional complexes. When exposed to laminar shear stress, endothelial cells activate and mobilize Ca^{2+} from intercellular stores. This mobilization leads to the formation of Ca^{2+}/calmodulin complexes, which then bind and activate the eNOS enzyme.[19] Furthermore, fluid shear stress induces the eNOS activation through the tyrosine phosphorylation of PECAM-1 (platelet endothelial cell adhesion molecule-1). This process enhances the phosphorylation of eNOS at Ser^{1177} and Akt Ser^{473} residues. In contrast, lower levels of activation are observed in static conditions in human umbilical cord vein endothelial cells (HUVECs).[20] Under laminar flow conditions, endothelial cells exhibit an atheroprotective phenotype. However, when laminar flow is disturbed or absent, the cells shift to an inflamed phenotype characterized by the activation of NF-κB.[21] This shift in phenotype can contribute to thermogenesis, inflammation, atherosclerosis,[22,23] and obstructive pulmonary disease.[24]

Given the crucial role of shear stress in accurately modeling physiological endothelial responses to risk factors, in vitro models must incorporate environmental cues such as laminar shear. This necessity is underscored by studies indicating that static endothelial cell-culture models exhibit a proinflammatory phenotype,[25] display features of complement-mediated injury,[26] and show impaired NO production.[27,28] When it comes to developing 3D models, microfluidics emerges as an optimal technology for introducing flow into a 3D microvascular structure.[25,29] The accurate measurement of NO poses a challenge due to its strong reactivity, short half-life, and low physiological concentrations. Traditional techniques such as the Griess assay, chemiluminescence, and amperometric NO sensor readings face limitations in accuracy and sensitivity.[30–34] However, measuring stable metabolites involved in NO production provides a viable approach to quantify NO, even at the low abundance in microfluidic cell models.

In particular, tracer-based metabolomics stands out as the gold standard method. This approach utilizes stable isotope-labeled precursors to trace complex pathways by following the labeled atom(s) to downstream metabolites.[35,36] This technique, applied to enzymatic reactions involved in NO production,[37–42] enhances accuracy and sensitivity, overcoming the challenges associated with traditional NO measurement methods. To evaluate the influence of adverse metabolic and inflammatory plasma factors on eNOS activity in both 2D and 3D endothelial cell models, we aimed to employ our tracer-based metabolomics strategy. In our study, we used $^{13}C_6$, $^{15}N_4$ L-arginine as a substrate for eNOS and traced its downstream metabolites $^{13}C_6$, $^{15}N_3$ L-citrulline (a co-product of NO production produced at equal molar amounts) and $^{13}C_5$, $^{15}N_2$ L-ornithine (contributing to citrulline production).

To assess these L-arginine downstream metabolites, we employed an optimized AccQ-Tag amino acid derivatization sample preparation method coupled with a targeted LCMS (liquid chromatography and mass spectrometry) approach. To validate the accuracy of our method in reflecting endothelial cell biochemistry, we measured changes in metabolite flux in cell models treated with stimulatory and inhibitory compounds for eNOS and arginase. Furthermore, we investigated the impact of unidirectional fluid flow on metabolic parameters associated with NO synthesis. This involved a comparison between a three-dimensional (3D) microvessels-on-chip model with controlled fluid flow[29,43] and a 2D static cell culture model. The results obtained highlight the suitability of the LCMS method for measuring low-volume and low-abundance NO downstream metabolites. Notably, the 3D

model reveals significant changes upon VEGF stimulation compared to the control situation, as evidenced by changes in Citrulline+9/Ornithine+7. In contrast, static 2D culture lacked significant changes upon VEGF stimulation, indicating a non-regulated eNOS and arginase pathway, reflecting an endothelial dysfunction condition. Furthermore, under flow conditions, there are elevated levels of mechanosensitive gene expression compared to static, low-shear, and bidirectional flow states. These results underscore the potential importance of shear stress and NO metabolite levels in influencing endothelial responses and gene expression patterns.

2 | MATERIALS AND METHODS

2.1 | Chemicals and reagents

Vascular Endothelial Growth Factor (VEGF) (PeproTech, Netherlands), L-NAME (Abcam, Netherlands), BEC (Sigma Aldrich, Netherlands), and BH4 (Merck, Netherlands) were used. RPMI SILAC – medium deficient in arginine was obtained from Thermo Fisher, Netherlands. Isotope-labeled L-Arginine was obtained from CORTECNET, Netherlands. Cells were grown under 5% CO_2, with 95% atmospheric air. Oxygen experiments were performed in a Panasonic 97 oxygen incubator. DAF-2D was obtained from Abcam, Netherlands.

2.2 | Cell culture and experimental procedures

Human coronary artery endothelial cells (HCAECs) (PromoCell, Netherlands) were resuspended in 10 mL fresh EGM MV2 medium with supplements (PromoCell, Netherlands) and cultured in T75 flasks (Nunc Easyflask, Sigma, Netherlands). Cell cultures were maintained at 37°C with 5% CO_2 and media was refreshed three times a week. Cells were detached at 85% confluence with 0.25% Trypsin EDTA (Lonza, Netherlands), and cell pellets were collected by centrifugation at 300 g for 5 min.

Commercially available RPMI SILAC medium was used, a formulation specifically designed for stable isotope labeling with amino acids in cell culture (SILAC). This medium lacks arginine, allowing for the incorporation of isotopically labeled L-arginine ($^{13}C_6$ $^{15}N_4$-L-arginine) at a concentration of 150 μM into the cells. Following treatment, we measured the downstream labeled metabolites in the cells. For 2D culture experiments, the collected cell pellets were suspended in a fresh medium to a concentration of 7×10^5 cells/ml and cultured in a 48-well plate for 48 h. The following day, cells were serum starved with 1%

FCS in basal EGM2 (Bioconnect, Netherlands) medium and incubated overnight. To synchronize or equilibrate the cell cycle, we treated cells with Krebs buffer solution, pH 7.4 (Thermo Fisher Scientific, Netherlands) for 1 h before the start of each experiment. Subsequently the cells were incubated for 12 h with RPMI SILAC (Thermo Fisher Scientific, Netherlands) supplemented with 150 μM $^{13}C_6$, $^{15}N_4$-L-arginine (CORTECNET, Netherlands), 10 μM of (6R)-5,6,7,8,-Tetrahydrobiopterin dihydrochloride (BH$_4$), and 1% FCS (Thermo Fisher Scientific, Netherlands) in the presence of 100 ng/mL VEGF, 1 mM L-NAME or 100 μM BEC separate or in the indicated combinations. The medium and cells were collected separately and snap frozen in liquid nitrogen and stored in −80°C for LCMS analysis.

For 3D cultures, we used a modified chip design 2-lane rerouted OrganoPlate (MIMETAS, Netherlands) that was adapted to attach a microfluidic pump to apply fluid flow and a normal 2-lane OrganoPlate to apply bidirectional flow. After seeding HCAEC cells into the 3D microvessels, they were cultured for 3–4 days with media refreshed every other day. Similar to the 2D culture, once the cells formed a microvessel, the following day, cells were serum starved with 1% FCS in basal EGM2 medium and incubated overnight. To synchronize or equilibrate the cell cycle, we treated cells with Krebs buffer solution, pH 7.4 for 1 h before the start of each experiment. Subsequently, the cells were incubated for 12 h with RPMI SILAC supplemented with 150 μM $^{13}C_6$, $^{15}N_4$-L-arginine, 10 μM of BH4, and 1% FCS in the presence of 100 ng/mL VEGF, 1 mM L-NAME or 100 μM BEC separate or in the indicated combinations. The medium and cells were collected separately, and snap-frozen in liquid nitrogen, and stored at −80°C for LCMS analysis.

The approximate cell count in each 2D plate well is in the range of $7–8 \times 10^3$ and in the 3D OrganoPlate the approximate cell count is in the range of $9 \times 10^3–1 \times 10^4$ cells/ chip (with 96 chips) per OrganoPlate.

2.3 | Immunofluorescence microscopy

HCAECs were fixed using 4% paraformaldehyde (PFA) in HBSS+ for 10 min at room temperature. The fixative was aspirated, and the cells were rinsed once with HBSS+. The cells were permeabilized for 2 min with 0.2% Triton X-100 in HBSS+ and washed with HBSS+. Permeabilization was followed by blocking cells using 5% BSA in HBSS+ for 30 min and then incubated with the primary antibody solution—Mouse anti-human CD144 (1:150) (BD Biosciences, USA) overnight at 4°C. The cells were washed with HBSS+, followed by a one-hour incubation with Hoechst (1:2000) (Invitrogen,

USA), rhodamine phalloidin (1:200) (Sigma-Aldrich, The Netherlands), and the secondary antibody solution, containing Alexa Fluor 488-conjugated goat anti-mouse (1:250) (Thermo Fisher, USA). The cells were washed three times with HBSS+. High-quality images of the stained cells were acquired using a high-content confocal microscope (Molecular Devices, ImageXpress Micro Confocal).

2.4 | Sample preparation for the LC–MS

Samples were analyzed using a method based on an amine profiling platform that employed an AccQ-Tag derivatization strategy, adapted from the protocol provided by Waters.[44] The cell-treated media and cell lysates (10 μL) were thawed on ice. For deproteination, water (5 μL), Tris-(2-carboxyethyl) phosphine hydrochloride (TCEP) (10 μL), and absolute methanol (75 μL) were added. Quality control (QC) samples were generated by pooling equal volumes of all cell media and cell lysate samples, and 10 μL of this pool underwent the same process as individual samples. After centrifugation at 13,200 rpm for 10 minutes, the supernatant was transferred to a fresh Eppendorf tube and dried under a speed vacuum. The dried residue was reconstituted in borate buffer (pH 9, 10 μL) vortexed for 10 s and treated with 2.5 μL of AccQ-Tag 5 μL AQC derivatization reagent (Waters, Waters B.V. Art. No. 186003836, The Netherlands). The samples were then kept at 55°C for 30 min in a shaker (Incubating microplate shaker, VWR, The Netherlands), 5 μL of 20% formic acid was added for neutralization. After a quick vortex, each sample was transferred to a deactivated autosampler vial for the LC–MS injection.

2.5 | Instrumentation and the LC–MS acquisition

Three microliters of the sample solution were injected onto a UPLC Class I (Acquity, Waters Chromatography Europe BV, Etten-Leur, The Netherlands) system with an AccQ-Tag Ultra C18 column (1.7 μm, 100 × 2.1 mm, Waters, Ireland) coupled to a Sciex QTRAP® 6500 mass spectrometer.[44] For liquid chromatography (LC) separation, mobile phase A consisted of 0.1% formic acid in water. Mobile phase B consisted of 0.1% formic acid in acetonitrile. The flow rate used was 0.7 mL/min and the starting gradient condition was 99.8% A for 0.5 min, changing linearly to 90% A over the next 5.50 min, 80% A over 7.50 min, 40% A at 8.00 min, 5.0% A at 9.00 min, after which the solvent composition returned to 99.8% A over next 9.10 min and ends up with 99.8% A and 0.2% B

over in next 11.00 min. Mass spectrometry experiments were carried out on a SCIEX QTRAP 6500. The ESI source parameters were as follows (positive ion mode): Spray voltage ±5.5 kV, capillary temperature 350°C, sheath gas 60 psi, auxiliary gas 70 psi, curtain gas 30 psi. Data acquisition was performed in scheduled multiple reaction monitoring mode targeting compounds with different labeling statuses. Q1 and Q3 resolutions for all transitions were set at unit resolution (0.7 amu FWHM) after testing with labeled cell samples. This setting was selective enough to reduce interference from adjacent ion peaks. The compound list with target m/z for parent and product ions is shown in Table S1. Raw LC–MS / MS data were processed using AB Sciex PeakView™ 2.0 and MultiQuant™ 3.0.1 software for targeted metabolite peak identification and integration. Metabolite isotopologue levels were quantified using the corresponding peak areas.

2.6 | Microfluidic pump setup

HCAECs were seeded into an OrganoPlate (similar protocol mentioned in the above section) that was specially designed for controlled perfusion using a pump attachment. The pump is made of stainless steel and the tube connections for the fluid transfer from the inlet and outlet of the chips are made of silicone. For controlled rotation, a small motor is operated with the help of LabVIEW solutions software. This software allows the control of fluid flow rate and related shear stress (dyne/cm^2), use of portal connections, motor position, and value. Typically, shear stress was applied for 12 h for metabolic readouts and 12 and 24 h for gene expression studies to condition the cells.

2.7 | Validation of eNOS activity using DAF-2DA

HCAECs were cultured in a 48-well plate with $7–8 \times 10^3$ cells/well suspended in a fresh EGM MV2 medium with supplements. Upon 80% confluence, the cells were starved with 1% FCS in EGM basal medium for 17 h at 37°C with 5% CO_2. Next, the cells were treated with Krebs buffer solution for 1 h at 37°C. After two washes of PBS, 5 μM of DAF-2DA stain (Abcam, Netherlands) was added and the cells were incubated for 1 h at 37°C and then washed twice with PBS. The cells were then treated with VEGF, L-NAME, BEC, and only the working solution (basal EGM2 media with 1% FCS and 10 μM BH_4) separately and incubated for 10–12 h as described previously. The cells were washed twice with PBS and

imaged in an EVOS CO_2 incubator-built fluorescent microscope with maximum excitation at 491 nm and maximum emission at 513 nm. The fluorescence intensities were measured by choosing ten random individual cells, and grayscale intensity was analyzed using the imageJ software to correlate with citrulline levels.

2.8 | Quantitative reverse transcription polymerase chain reaction (RT-PCR)

To perform RT-PCR, cells from 2D wells and OrganoPlate chips were collected by adding 100 μL of RLT buffer (QIAGEN, Netherlands); after 60 seconds of incubation at RT the lysates were collected, and RNA was extracted using Qiagen's RNAeasy kit and Buffer RLT lysis buffer based on the manufacturer's recommendations. Next, to enable analysis of gene expression at low concentrations due to low cell counts, the lysate of eight microvessels from 3D cell culture models and eight well samples from 2D-48 well plates were combined to make one sample. Reverse transcription-mediated cDNA synthesis was carried out using random and oligo(dT) primers (Bio-Rad, Netherlands) in accordance with the manufacturer's instructions using 200 ng of total RNA. For the qRT-PCR analysis, SYBR Select (Invitrogen) and a Biorad CFX384 were utilized. Krüppel-like transcription Factor2 (Klf2) (sense), CTACACCAAGAGTTCGCATCTG; Klf2 (antisense), AGCACGAACTTGCCCATCA; 18S rRNA (sense), GGATGTAAAGGATGGAAAATACA; 18S rRNA (antisense), TCCAGGTCTTCACGGAGCTTGTT were the target genes whose primer sequences were employed. Expression levels were standardized to 18S rRNA and quantified using the comparative cycle threshold (ΔΔCt) method.

2.9 | Statistical analysis

Bar plots and box plots were created using GraphPad Prism 9.3.1 software. Significance was determined by ANOVA, Tukey's analysis, and student's *t*-test.

3 | RESULTS

The method for measuring eNOS activity in 2D cell culture was first optimized and validated using isotope-labeled arginine, the LC–MS /MS analysis, and staining using DAF (Sections 3.1–3.4). Next, the method was also optimized for the 3D microvessels-on-chip model (Section 3.5), and finally, the eNOS activity was measured for the 2D and 3D microvessels-on-chip model (Section 3.6).

3.1 | Tracer-based measurement of eNOS-dependent arginine to citrulline conversion: Marker metabolites that reflect eNOS activity

The targeted analysis of isotope-labeled L-arginine and its downstream metabolites, L-citrulline and L-ornithine, was conducted using the sample preparation method involving AccQ-Tag derivatization. The metabolic pathway of L-arginine metabolism and its conversion to downstream metabolites, as illustrated in (Figure 1A), was the focal point of our analysis. We optimized the method by analyzing potential isotopologues of these marker metabolites in the cell system (Table S1).

After treating the HCAECs with isotope-labeled L-arginine, we analyzed the resulting samples to identify peaks representing a series of isotopomeric citrulline, arginine, and ornithine in the reconstructed ion chromatograms (Figure 1B). Arginine was detected with M + 10 (representing $^{13}C_6$, $^{15}N_4$ labeling) as a primary isotopologue, accounting for over 60% of $^{13}C_6$ $^{15}N_4$ L-arginine in all samples. Citrulline was detected with M + 9 (representing $^{13}C_6$, $^{15}N_3$) as the primary isotopologue, produced by losing one nitrogen. Ornithine was detected with M + 7 (representing $^{13}C_5$, $^{15}N_2$), resulting from the loss of one carbon and two nitrogen atoms from arginine. In the subsequent analysis, $^{13}C,^{15}N$-arginine (M + 10), $^{13}C,^{15}N$-citrulline (M + 9), and $^{13}C,^{15}N$-ornithine (M + 7) were selected as biomarkers for further investigation. The measurements of blank samples (only media) showed no background interference in isotope-labeled citrulline or ornithine peaks (results not shown).

To optimize the incubation time, we considered the effects observed with stimulatory and inhibitory compounds. We utilized the detected isotopologues to verify the uptake of $^{13}C_6$, $^{15}N_4$ L-arginine and reconstruct the metabolic pathways controlled by eNOS and arginase in HCAECs. This analysis encompassed four conditions: (1) control; (2) treatment with the stimulatory compound VEGF, known for inducing NO release from endothelial cells[45]; (3) treatment with the eNOS inhibitory compound L-NAME[46,47]; and (4) treatment with the arginase enzyme inhibitor BEC.[48] The pathway and resulting metabolite expression for each treatment are depicted in Figure 2A–C. The optimization process led us to select a 12-h incubation time after the introduction of tracers. We observed lower labeling incorporation at 3 and 6 h, as indicated by the ratio of citrulline+9/arginine+10 and ornithine+7/arginine+10 (Figure S1).

This rate of label incorporation could be influenced by the exchange of intracellular and extracellular (in medium) metabolites. Thus, we opted for a 12-h treatment to see a maximal transfer of ^{13}C and ^{15}N atoms. The
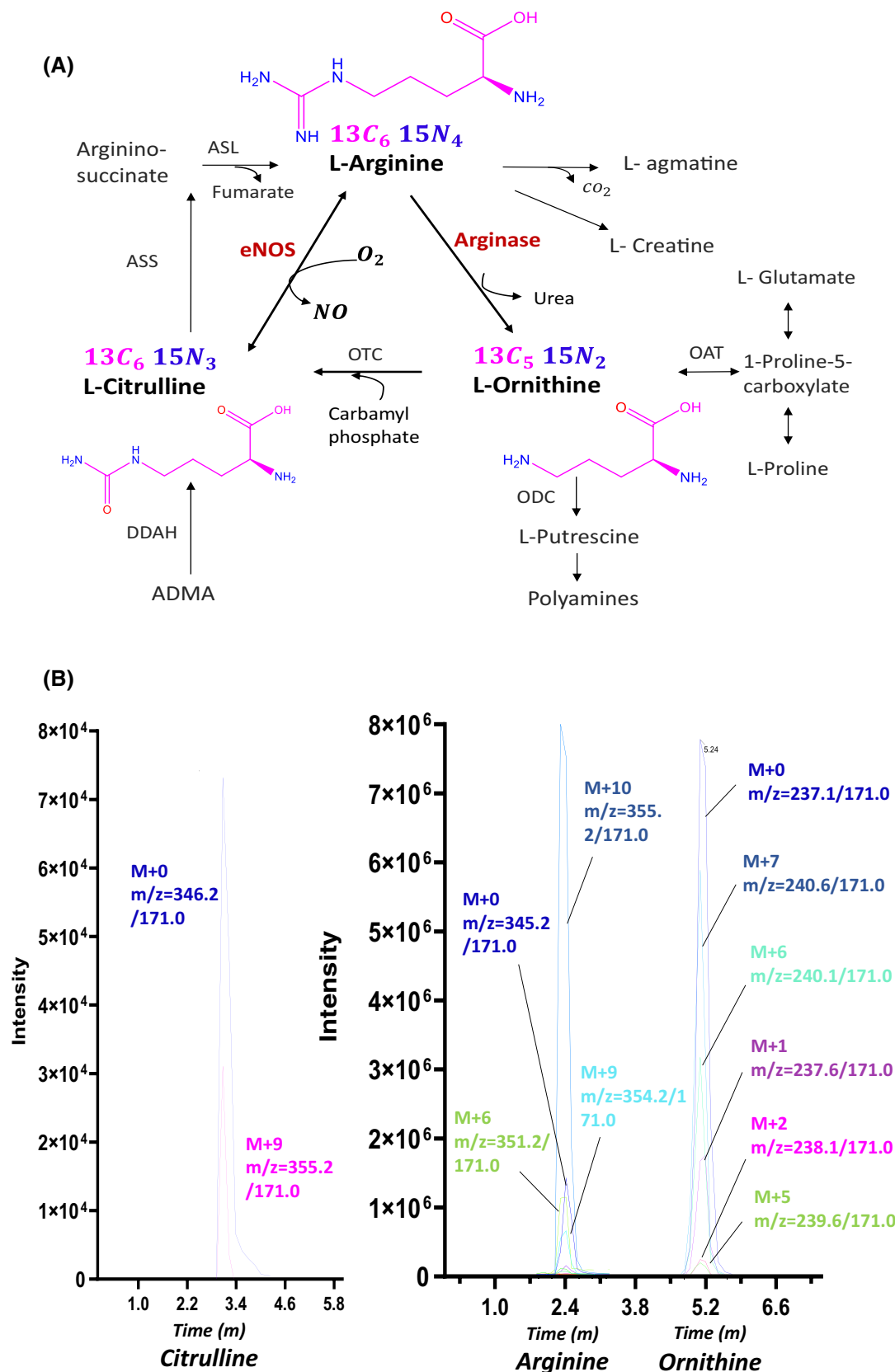
FIGURE 1 Tracer-based Nitric Oxide (NO) metabolomics study. (A) Metabolic pathway of L-arginine and a few metabolites involved in other functions. Three marker metabolites (in bold) were analyzed based on stimulated and inhibited conditions of the respective enzymes eNOS and arginase. (B) Representative ion chromatograms of metabolite isotopologues detected in the HCAECs samples were obtained after cells were incubated with 150 μM of $^{13}C_6$ $^{15}N_4$ L-arginine.
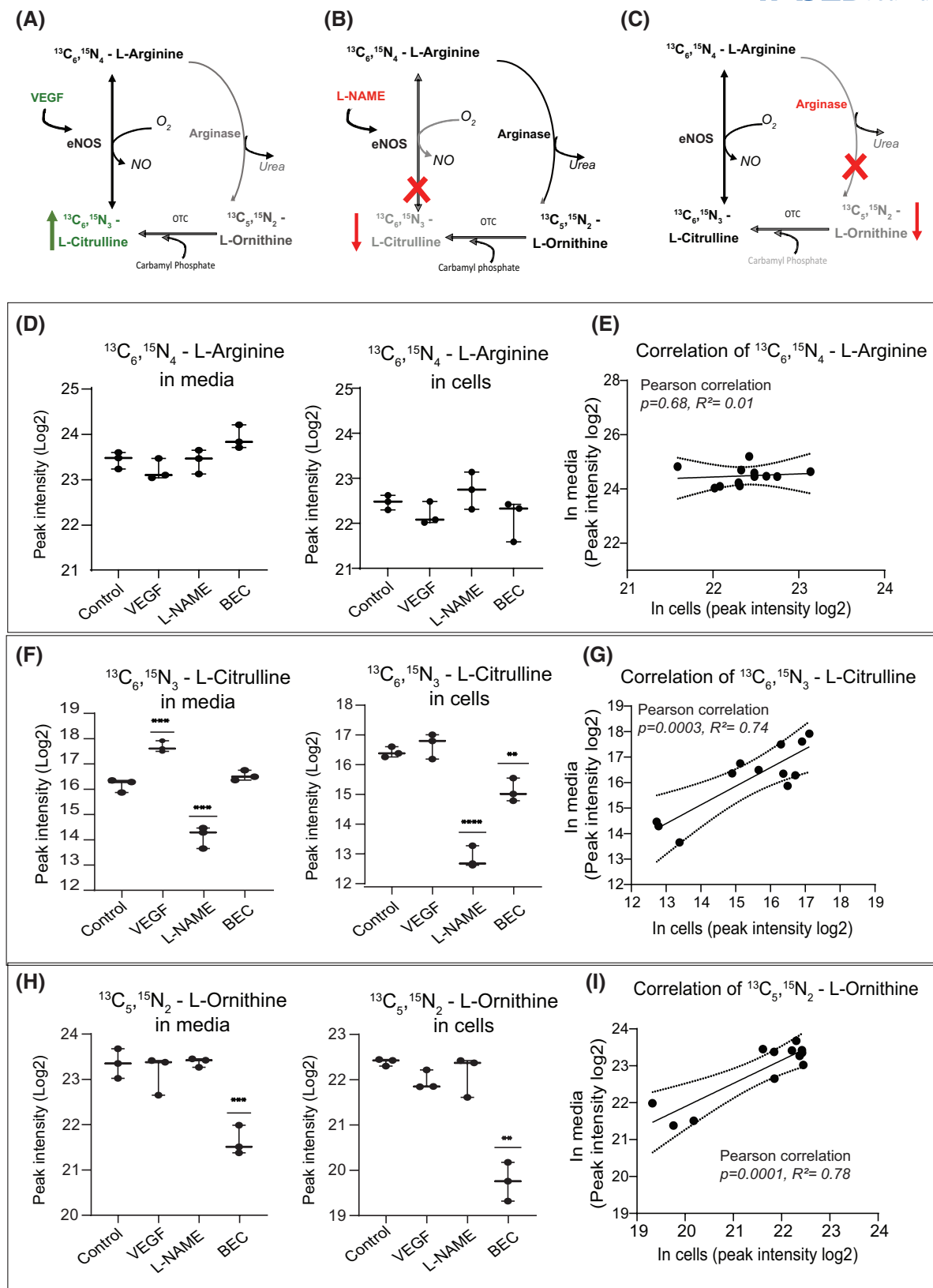
FIGURE 2 Measurement of isotope-labeled extracellular (media) and intracellular (cells) marker metabolites involved in NO mechanism in 2D model. (A) Schematic representation of NO pathway upon treatment of (A) VEGF—eNOS stimulation, (B) L-NAME—eNOS inhibition, and (C) BEC—arginase inhibition. Highlighted and non-highlighted paths represent activation and inhibition conditions. Measurement of metabolites in media and cells (D) $^{13}C_6$, $^{15}N_4$ L-arginine and its (E) Pearson correlation (F) $^{13}C_6$, $^{15}N_3$ L-citrulline and its (G) Pearson correlation (H) $^{13}C_5$, $^{15}N_2$ L-ornithine and its (I) Pearson correlation. All error bars represent SD and mean, each dot represents technical replicates, $n = 3$. Significance determined by student t-test of treated group versus control group. $*p < .05$; $**p < .01$; $***p < .001$; $****p < .0001$.

calculated isotopologue fractions after 12 h of incubation time show the utilization of labeled arginine converted into maximum transition state of labeled citrulline (M + 9) and ornithine (M + 7) in extracellular samples.

In intracellular samples, the degree of labeling (citrulline (M + 9) and ornithine (M + 7) compared to the unlabeled isotopologue) was lower than in the medium (Figure S2A,B). While the precise reason for this remains unclear, the suppression of citrulline generation by L-NAME is evident in both media and cells. Additionally, the hindrance of ornithine production by BEC is also distinctly observed in both media and cells. Indeed, the collective impact (notably, the isotopologue fraction of labeled citrulline (M + 9)) is more pronounced in the medium.

3.2 | Extracellular and intracellular measurement of Isotopomeric compounds

In order to comprehensively understand the effects of stimulatory and inhibitory compound treatments and to evaluate cellular metabolism, we conducted measurements of marker metabolites both intracellularly and extracellularly in a 2D cell culture platform. HCAECs were treated with eNOS stimulator (VEGF), eNOS inhibitor (L-NAME), and arginase inhibitor (BEC) in conditioned media containing $^{13}C_6$, $^{15}N_4$ L-arginine for 12 h. Subsequently, both extracellular (media) and intracellular (cell) samples were analyzed with the LC–MS /MS. The targeted metabolic routes for individual treatments are illustrated in (Figure 2A–C).

$^{13}C_6$, $^{15}N_4$ L-arginine was present in a high amount in the medium and was also high in the cell. VEGF, L-NAME, and BEC did not change the labeled arginine level significantly in media or cells, and that is not unexpected due to the high level as substrate (Figure 2D), and as the levels were rather constant in cell and medium for the various conditions, no significant correlation was found for values of $^{13}C_6$, $^{15}N_4$ L-Arginine (Pearson correlation coefficient p value = .6, R^2 = .01) (Figure 2E).

The peak intensity of $^{13}C_6$, $^{15}N_3$ L-Citrulline in the medium was increased in VEGF when compared to control but no statistical difference was observed in the cells (Figure 2F).

The eNOS inhibition with L-NAME treatment shows significantly lower $^{13}C_6$, $^{15}N_3$ L-Citrulline in cells and media, while with arginase inhibition, the levels were not significantly changed. Overall, our results show that there is a significant positive correlation between media and cells for $^{13}C_6$, $^{15}N_3$ L-Citrulline (Pearson correlation coefficient, p = .0003, R^2 = .7) (Figure 2G). The $^{13}C_5$, $^{15}N_2$ L-Ornithine levels were not significantly affected by VEGF and

L-NAME treatments, in contrast to the condition where a specific inhibition of the arginase enzyme with BEC treatment was added, resulting in decreased ornithine levels (Figure 2H). When we measured $^{13}C_5$, $^{15}N_2$ L-Ornithine in media and cells, a significant positive correlation with p value = .0001, R^2 = .7 was observed (Figure 2I).

3.3 | Analysis of metabolic ratios to understand NO metabolic flux

Employing the tracer-based extracellular measurement method highlighted earlier, our emphasis was on ratios indicative of metabolic fluxes. We conducted inquiries involving both individual and combined treatments of endothelial cells with compounds that stimulate and inhibit eNOS and arginase enzymes.

Under eNOS stimulation conditions (VEGF, Pathway Figure 2A) the expected outcome is a maximized production of citrulline compared to conditions involving arginase and eNOS inhibition (Pathway Figure 2B,C). The ratio $^{13}C_6$, $^{15}N_3$ L-citrulline/$^{13}C_6$, $^{15}N_4$ L-arginine was found to be significantly higher in the VEGF treatments, indicating a greater utilization of arginine for citrulline conversion (Figure 3A). The $^{13}C_6$, $^{15}N_3$ L-citrulline/$^{13}C_5$, $^{15}N_2$ L-ornithine ratio serves as an indicator of the balance in the metabolic pathway associated with arginase and eNOS activities. Our results show a significant increase is observed in arginase inhibition conditions (BEC and VEGF+BEC) (Figure 3B). The inhibition of eNOS by L-NAME treatments (L-NAME and VEGF+L-NAME) (Figure 3B) led to lower levels of citrulline and $^{13}C_6$, $^{15}N_3$ L-citrulline/$^{13}C_5$, $^{15}N_2$ L-ornithine ratio indicating that the eNOS inhibition was selective.

The $^{13}C_5$, $^{15}N_2$ L-ornithine/$^{13}C_6$, $^{15}N_4$ L-arginine ratio, analyzed to confirm the utilization of arginine to ornithine conversion, showed lower expression in all arginase inhibition (BEC) conditions compared to other treatments (Figure 3C).

3.4 | Validation of eNOS activity using NO specific DAF-2DA staining

To determine if citrulline production can serve as an estimate of eNOS activity, we compared the peak intensities of $^{13}C_6$, $^{15}N_3$ L-citrulline with another measure of eNOS activity—diaminofluorescein-2 diacetate (DAF-2DA) fluorescence staining for detecting intracellular NO. When DAF-2DA is taken up by cells, cytoplasmic esterase cleaves the acetate groups to generate DAF-2 which can readily react with dinitrogen trioxide (N_2O_3), an oxidation product of NO, to form the highly fluorescent triazolo fluorescein (DAF-2T) (Figure 4).

(A)

$^{13}C_6, ^{15}N_3$ - L-Citrulline/$^{13}C_6, ^{15}N_4$ - L-Arginine

(B)

$^{13}C_6, ^{15}N_3$ - L-Citrulline/$^{13}C_5, ^{15}N_2$ -L-Ornithine

(C)

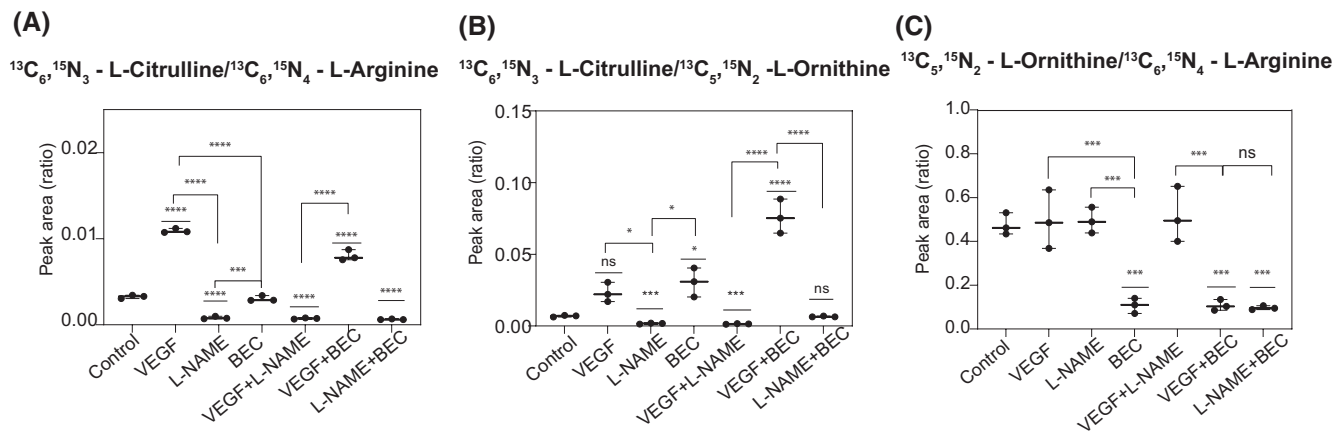$^{13}C_5, ^{15}N_2$ - L-Ornithine/$^{13}C_6, ^{15}N_4$ - L-Arginine

FIGURE 3 Measurement of extracellular labeled metabolites in 2D platform with the treatment of stimulators and inhibitors in individual and combinational treatments. (A) Ratio of $^{13}C_6$, $^{15}N_3$ L-citrulline/$^{13}C_6$, $^{15}N_4$ L-arginine, (B) ratio of $^{13}C_6$, $^{15}N_3$ L-citrulline/$^{13}C_5$, $^{15}N_2$ L-ornithine, and (C) ratio of $^{13}C_5$, $^{15}N_2$ L-ornithine/$^{13}C_6$, $^{15}N_4$ L-arginine. All error bars represent SD and mean, each dot represents biological replicates. Significance was determined by ANOVA and Tukey's multiple comparison test. ns = not significant; $*p < .05$; $**p < .01$; $***p < .001$; $****p < .0001$.

(A)

(B)

DAF-2T fluoresence intensity

(C)

Correlation of $^{13}C_6, ^{15}N_3$ - L-Citrulline and DAF-2T

Spearman correlation
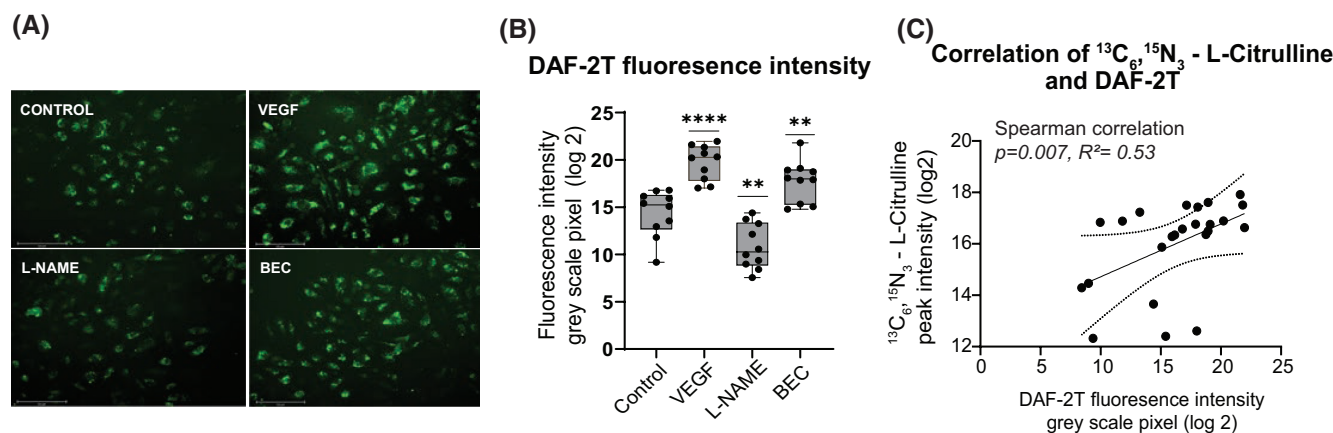*p=0.007, R²= 0.53*

FIGURE 4 NO specific DAF-2 DA fluorescent stain on HCAECs. (A) Microscopic images of HCAECs using fluorescent NO stain DAF-2DA in all treatments; eNOS stimulator (VEGF), inhibitor (L-NAME), and arginase inhibitor (BEC). (B) The intensity of the fluorescent stain was calculated by grayscale measurement using ImageJ software; $n = 10$. (C) Spearman correlation of $^{13}C_6$, $^{15}N_3$ L-citrulline, and DAF-2T fluorescence intensity. Significance determined by student t-test. ns = not significant; $*p < .05$; $**p < .01$; $***p < .001$; $****p < .0001$.

This experiment was conducted in the 2D platform (48 wells cell culture plate) under the same conditions used for metabolic readout as described in the preceding section. DAF-2T fluorescence intensity is significantly higher in VEGF and BEC conditions, and lower intensity was observed in the L-NAME condition (Figure 4A,B). This outcome aligns with observations indicating that VEGF stimulation leads to a simultaneous increase in $^{13}C_6$ $^{15}N_3$ L-citrulline peak intensity (Figure 2F media) and the augmentation of DAF-2T signals in HCAECs (Figure 4B). To compare the relation between NO level and citrulline production, we performed a correlation analysis. Overall, the statistical analyses of the data indicate a significant correlation between DAF-2T fluorescent intensity vs. $^{13}C_6$ $^{15}N_3$ L-citrulline peak intensity (Spearman correlation coefficient, $p = .007$, $R^2 = .53$) indicating that $^{13}C_6$ $^{15}N_3$

L-citrulline production and NO production from the 2D model is significantly linked to the eNOS controlled treatments (Figure 4C). Results from the DAF-2DA stain in the 3D model were inconclusive due to the presence of the collagen matrix. This matrix caused high background staining, making it difficult to distinguish the specific signal from the endothelial cells. Hence the results were not shown.

3.5 | Comparison of mechanosensitive Klf2 gene in static (2D) and flow-mediated (3D) cell culture models

To investigate the importance of shear stress on eNOS activation at the gene and metabolic level, we used a 3D

culture model utilizing a novel setup—the MIMETAS 2-lane rerouted OrganoPlate (Figure 5A). The commercially available MIMETAS 2-lane OrganoPlate chip design was altered (rerouted) by connecting the route of windows 1 and 4 (Figure 5B), extending the surface area for more cell growth. More importantly, this design is suitable to connect our microfluidic pump to create a flow, in contrast to the commercial MIMETAS OrganoPlate, where such a connected route is not present, as flow is applied using the rocker platform that generates bidirectional flow.[29] The microchannels in the OrganoPlate for gel and perfusion (blue-1 and pink-2 channel) are illustrated in Figure 5C. The microchannels in the OrganoPlate were coated with gelatin, preventing HCAECs from growing on glass and enabling them to form stable microvessels which were checked by immunostaining (Figure 5D). The rerouted OrganoPlate was connected to the microfluidic pump as shown in Figure 5E.

For this study, we utilized three different cell culture models: (a) the 2D model in which cells were grown in a static conventional culture, (b) a bidirectional flow model—MIMETAS 2-lane OrganoPlate with normal chip design subjected to flow using an interval rocker device,[29] and (c) a unidirectional flow model—the rerouted plate with microfluidic pump set to two different dyne stresses, namely, 0.3 and 5.0 dyne/cm^2. From these platforms, HCAECs were collected, and RNA was isolated at 12 and 24 h. The isolated RNA was transcribed to cDNA with the respective primers and quantified using the RT-PCR technique.

The results of the 12-h incubation reveal a significant upregulation of the Klf2 gene in microvessels perfused with the interval rocker and with the microfluidic pump (5 dyne/cm^2).

Furthermore, the results of the 24-h incubation demonstrate that cells subjected to perfusion with the interval rocker platform exhibit a significant upregulation of the Klf2 gene compared to cells in the 2D well plate, and microvessels perfused with the pump may exhibit a further increase in Klf2 gene expression (Figure 5F).

3.6 | Comparison of NO marker metabolites in static (2D) and flow-mediated (3D) cell culture models

Metabolic analysis was performed in the samples obtained from the above-mentioned models (in Sections 3.2 and 3.3), and ratios of $^{13}C_6$, $^{15}N_3$ L-Citrulline, $^{13}C_5$, $^{15}N_2$ L-Ornithine, and $^{13}C_6$, $^{15}N_4$ L-arginine were evaluated. The ratio of $^{13}C_6$, $^{15}N_3$ L-citrulline/$^{13}C_6$, $^{15}N_4$ L-arginine and $^{13}C_5$, $^{15}N_2$ L-ornithine/$^{13}C_6$, $^{15}N_4$ L-arginine are higher for 2D than 3D experiments, indicating that the total eNOS and arginase activity is higher in 2D than 3D. More relevant, the ratio of labeled citrulline and ornithine is higher for 3D than 2D, indicating that the ratio of eNOS activity to arginase activity is higher for 3D than 2D, which is expected due to the flow present in 3D (Figure 5G).

The metabolic effects of VEGF, L-NAME, and BEC treatments were comparable between 2D and 3D cultures for the above-mentioned ratios (Figure S4A–C). However, the $^{13}C_6$, $^{15}N_3$ L-citrulline/$^{13}C_5$, $^{15}N_2$ L-ornithine ratio showed a significant increase in all the 3D models when eNOS was stimulated by VEGF but was not significantly higher in 2D culture compared to control (Figure S4A).

4 | DISCUSSION

The purpose of this study was to understand endothelial NO production from a metabolic standpoint. We examined isotope-labeled arginine-based NO metabolic modifications by employing specific stimulant and inhibitory compounds targeting eNOS and arginase enzymes. Our focus was on measuring the impact of adverse metabolic and inflammatory factors on NO synthesis in endothelial cells, and for this purpose, we developed a highly sensitive tracer-based method to quantify the eNOS-dependent conversion of arginine to citrulline and ornithine.

Upon introducing the arginine isotope to the HCAECs, we optimized the time required for the conversion of

FIGURE 5 Representation of our 3D blood vessel model and a comparison of NO marker metabolites in 2D and 3D platforms. (A–C) Illustration of re-routed OrganoPlate's single-chip design; every microfluidic chip structure is positioned underneath four adjacent wells. Each microfluidic chip consists of two channels: The blue color represents a "perfusion" channel and the pink color represents a "gel" channel (ECM) separated by a phase guide (*). Every first well (1) and fourth well (4) is positioned on top of the inlet and outlet of the perfusion channel, while every second well (2) is for the gel channel and every third well (3) is used for imaging and observation of the experiment. (D) Immunostaining of HCAECs in a chip. After 48 h of cell seeding, confluent vessels of HCAECs were immunostained with V-cadherin, actin, and DAPI. (E) Image of a microfluidic pump with the two metal tubes attached to the inlet and outlet of the rerouted OrganoPlate to carry fluid and create unidirectional flow. (F) Measurement of KLF2 gene expression of cell samples and (G) measurement of extracellular metabolite's ratio—$^{13}C_6$, $^{15}N_3$ L-citrulline/$^{13}C_5$, $^{15}N_2$ L-ornithine, $^{13}C_6$, $^{15}N_3$ L-citrulline/$^{13}C_6$, $^{15}N_4$ L-arginine, $^{13}C_5$, $^{15}N_2$ L-ornithine/$^{13}C_6$, $^{15}N_4$ L-arginine, all obtained from 2D static (black bars), 3D rocker platform (bidirectional flow model—blue bars) and the rerouted OrganoPlate with microfluidic perfusion pump operated with different shear stresses (unidirectional flow model) 0.3 dyne/cm^2—(brown bars), 5 dyne/cm^2 (green bars). Data for RT-PCR are presented as mean and s.e.m; $n = 3$. Metabolic data significance determined by one-way ANOVA multiple comparison tests. *$p < .05$; **$p < .01$; ***$p < .001$; ****$p < .0001$.
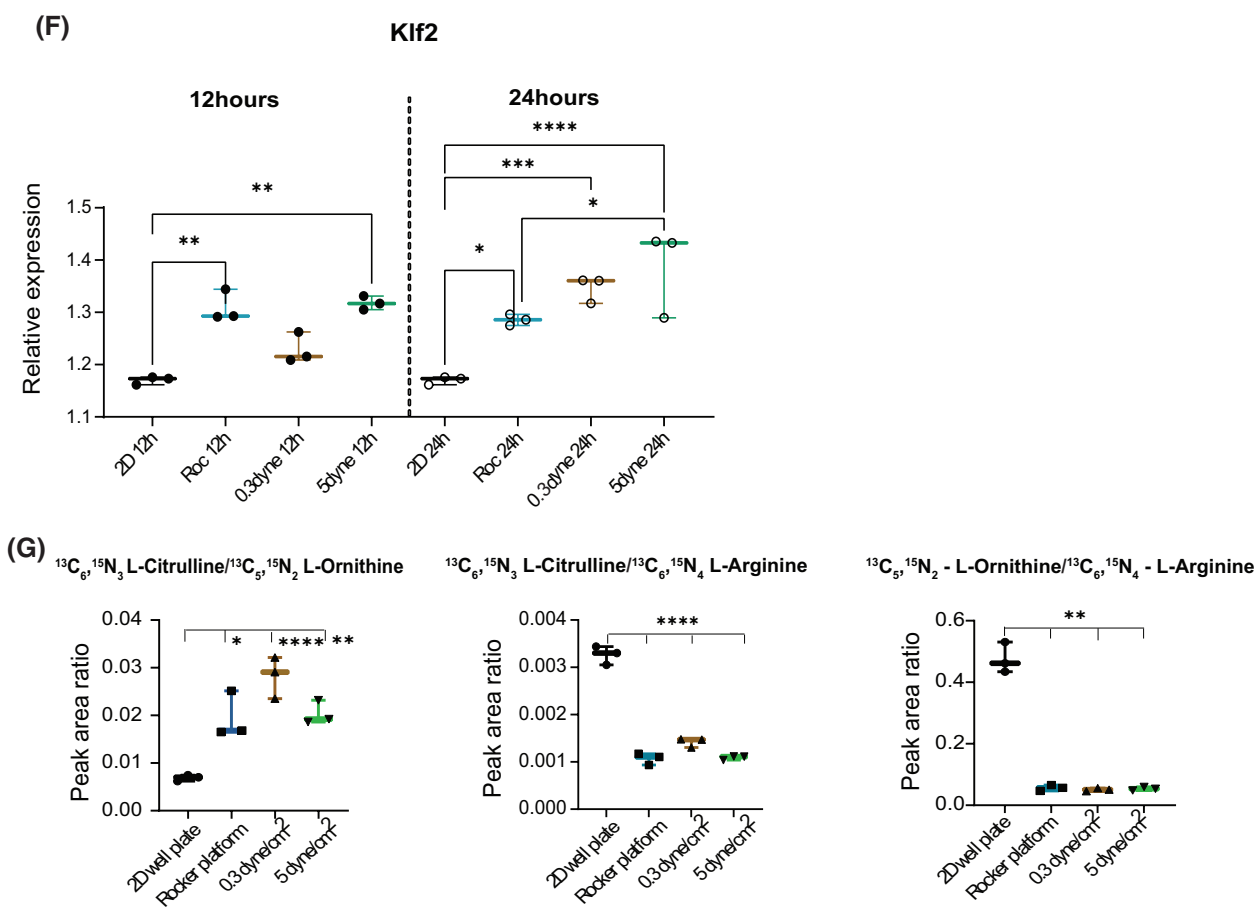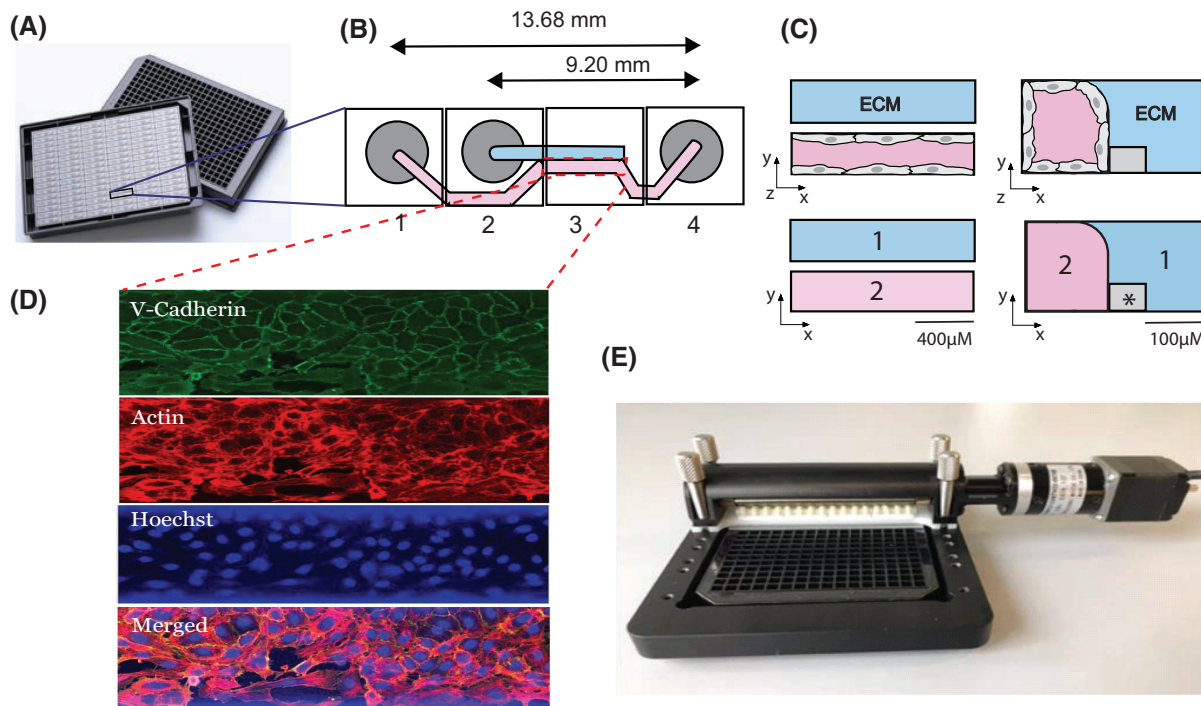
isotope-labeled citrulline and ornithine. Through the optimization process, we determined that a 12-h incubation period after tracer introduction yielded the most favorable results. Notably, lower labeling incorporation was observed at 3 and 6 h, as evidenced by the citrulline+9/arginine+10 and ornithine+7/arginine+10 ratios (Figure S1).

The incorporation rate of labels may be impacted by the exchange of metabolites between intracellular and

extracellular (in medium) environments. Consequently, we chose a 12-h treatment to observe the maximal transfer of 13C and 15N atoms. The calculated isotopologue fractions following a 12-h incubation period reveal the utilization of labeled arginine, leading to the maximum transition state of labeled citrulline (M + 9) and ornithine (M + 7) in extracellular samples. In intracellular samples, the degree of labeling (citrulline (M + 9) and ornithine (M + 7) compared to the unlabeled isotopologue) was lower than in the medium (Figure S2A,B).

Upon introducing the isotope-labeled arginine to the HCAECs and when treated with stimulatory and inhibitory compounds, it can be inferred that discernible (relative, not absolute) variations in eNOS and arginase activities can be identified through the assessment of the M + 9 isotopologue of citrulline and M + 7 ornithine in the medium. Additionally, it is imperative to emphasize that when evaluating the impact of conditions on eNOS activity, a control experiment must be incorporated as a reference. Moreover, a notable abundance of the M + 6 isotopologue in arginine is observed, attributed to its conversion through an alternative pathway. It was concluded that the obtained labeled marker metabolites were relatively high after 12 h in the medium; therefore, further analyses were performed on medium samples produced after 12 h of incubation.

The response of eNOS stimulation using VEGF was to enhance the NO production through the activation of tyrosine kinase activity, resulting in the phosphorylation of intracellular domains. This activation increases calcium levels, facilitates binding with calmodulin (CaM), enhances eNOS phosphorylation, and ultimately leads to increased NO production.[49–52] The mechanism via receptor activation is depicted in Figure S3. Our results indicate that eNOS activation leads to increased citrulline, consistent with its role as a co-product of NO production.

Earlier studies have reported BEC as a classical competitive inhibitor of arginase II at pH 7.5 with a dissociation constant (Ki) describing the binding affinity between the inhibitor and the enzyme as 0.25 and 0.31 μM.[53] Therefore, both citrulline and ornithine, upon stimulatory and inhibitory compound exposures, exhibited similar effects between media and cells. In general, most of the in vitro analyses measured NO metabolites only as intracellular levels.[54,55] In our study, we showed that the obtained promising results showed extracellular and intracellular expressions are positively correlated and this approach is helpful for fluxomics studies.

Ratios of NO metabolites can function as valuable indicators of diseased conditions and are considered useful markers in cardiovascular diseases, offering insights into the underlying biological mechanisms and disrupted pathways associated with the disease state. In particular, the tracer-based approach allowed us to gain a comprehensive understanding of how these compounds, both individually and in combination, influence the metabolic pathways associated with endothelial dysfunction. The ratio of unlabeled citrulline to arginine has been extensively examined in diabetes condition[56] and in children with chronic kidney disease (CKD) and abnormal cardiac blood pressure conditions, reporting a higher citrulline-to-arginine (cit-arg) ratio in plasma[57] but a lower ratio reported in urine.[58] In our study using stable isotope ratios instead of unlabeled ratios, we were able to overcome the difficulties resulting from the large volume of media used compared to the cell content and clearly link the arginine substrate to downstream products. The higher ratio resulting from the BEC inhibition suggests that arginase inhibition could be a potential target for recovering NO or citrulline production in diseased conditions. Our data supports the idea that the arginase inhibition recovers citrulline levels better than the stimulated condition with more arginine availability.[59]

Furthermore, the combinational exposure experiments provide insights into the metabolic alterations in a controlled fashion. For instance, under VEGF+BEC conditions, production of $^{13}C_6$, $^{15}N_3$ L-citrulline was directly from arginine rather than from ornithine as the pathway is blocked by the arginase inhibitor BEC. Such information is valuable for comparing the underlying mechanisms of disease and identifying potential targets for therapeutic interventions.

Measurement of DAF-2T, the NO-specific stain, revealed higher florescent intensity for both VEGF and BEC conditions which indicates an enhancement of NO production with VEGF addition, as previously demonstrated in HUVEC cells.[60] Similarly, increased DAF-2T intensity in arginase inhibition indicated the restoration of NO production, consistent with what was reported earlier in human aortic endothelial cells (HAECs).[61] After the successful use of the DAF-2T staining in the 2D HACEC model, we evaluated the staining in the 3D microvessels model. However, direct staining was not successful, with the major challenge that the dye showed a too strong background signal when reacting to the collagen which was used as the extracellular matrix in the 3D microvessels model (results not shown). Therefore, to confirm the impact of flow that creates change in isotope-labeled citrulline peak levels in 3D model, the flow-sensitive gene expression was measured.

Endothelial response to fluid flow is a crucial factor in vascular regulatory function. Flow-mediated eNOS

activity in endothelium releases the endogenous nitro vasodilator, NO.[17,62,63] We validated the functionality of our microfluidic pump, using quantitative RT-PCR to measure the impact of shear stress on the shear-dependent transcription of the Klf2 gene[64] which also plays an important role in endothelial function, anti-inflammatory, anti-thrombotic, and angiogenesis.[63,65] This indicates that our flow model induces substantial upregulation of the shear-dependent gene—Klf2, highlighting the effectiveness of our 3D model in providing proper flow conditions to cells and allowing variations in shear stress compared to 2D.

The advantage of comparing ratios of 2D and 3D models rather than comparing individual metabolites is that ratios eliminate the need for additional normalization methods such as cell count or protein levels for some (but not all) comparisons. The ratio of $^{13}C_6$, $^{15}N_3$ L-citrulline/$^{13}C_6$, $^{15}N_4$ L-arginine and $^{13}C_5$, $^{15}N_2$ L-ornithine/$^{13}C_6$, $^{15}N_4$ L-arginine is higher for 2D than 3D experiments, indicating that the total eNOS and arginase activity is higher in 2D than 3D, but this may be due to the higher number of cells in the 2D model. The influence of flow is evident in the $^{13}C_6$, $^{15}N_3$ L-citrulline/$^{13}C_5$, $^{15}N_2$ L-ornithine ratio, indicating that flow "regulates" metabolic expression by enhancing eNOS activity when compared to the static 2D model. This might be because the cells in the 2D model undergo stress due to the stiff base substrate and a static culture method, which mimics the status of endothelial dysfunction. These findings support the hypothesis of a relative arginase hyperactivity leading to endothelial dysfunction (ED) in mice[66] and in diabetic patients with ED.[67] Furthermore, the loss of fluid flow combined with an mTOR-based regulatory mechanism to balance eNOS and arginase II expression results in elevated $^{13}C_5$, $^{15}N_2$ L-ornithine and decreased $^{13}C_6$, $^{15}N_3$ L-citrulline levels, which indicates ED, consistent with what was reported in these studies.[68,69]

Flow-induced increases in NO production compared to static culture were previously reported.[70] Our results also show similar findings that in a 3D flow model, the fluid shear stress induces the signal of PECAM-1 that acts through adaptor molecules such as phosphatidylinositol-3-kinase (PI3K), which then activates eNOS, mTOR, and the transcription factor Klf2 to regulate the functional genes.[63] Therefore, a lower $^{13}C_6$, $^{15}N_3$ L-citrulline/$^{13}C_5$, $^{15}N_2$ L-ornithine ratio in 2D static culture mimics more of endothelial dysfunction conditions. With the microfluidic pump, the flow can be controlled; for the $^{13}C_6$, $^{15}N_3$ L-citrulline/$^{13}C_5$, $^{15}N_2$ L-ornithine ratio, the data for the rocker platform and microfluidic platform using a shear stress of 5 dyne/cm^2 were not statistically significant.

5 | CONCLUSION

We developed a stable isotope LC–MS/MS-based assay to determine eNOS activity and verified this method by showing that indeed eNOS expression was present with reference staining (DAF-2DA), and inhibitors of eNOS and arginase did show the expected effect. We then used this method to measure the eNOS activity of HCAECs in 2D culture, and in a 3D microvessels model with flow through the microvessels. We used a bidirectional flow and a setup with a unidirectional flow system generated by a microfluidic pump. Compared to 2D culture, the 3D model has higher eNOS activity. Additionally, our optimized MS method proves to be ideal for measuring NO marker metabolites at both extracellular and intracellular levels, providing valuable insights into metabolic flux. The method can be used to determine the effect of medium or plasma perfusion through the microvessels on eNOS activity by measuring the conversion of labeled arginine to citrulline in the medium (extracellular), which is much more straightforward than extracting endothelial cell content. This eNOS activity assay has advantages over fluorescent probes which may have background interference from the extracellular matrix and it offers the potential to be faster and high throughput as lysis of cells is not necessary and can be conducted at several time points throughout an experiment.

In future studies, this method could be applied to assess the effect of patient plasma on eNOS activity by perfusing patient plasma samples in the 3D models and analyzing the degree of pathological conditions and drug responses. Combining flux data with other omics data in future studies would offer a more comprehensive understanding of NO's vasodilatory effects in studying endothelial dysfunctions. Furthermore, enhancing the pump system with higher shear forces could be explored to apply to various endothelial cell types, emulating different microvessel models. In conclusion, our validation of shear stress's impact on eNOS using our 3D cell culture model from a metabolic perspective is a novel approach to studying endothelial (dys)function.

ACKNOWLEDGMENTS

DISCLOSURES

During the preparation of this manuscript, the author(s) used ChatGPT 3.5 (on March 2024) to assist with language correction and to improve the readability of the text. The content and scientific interpretations presented in this manuscript are entirely the work of the authors. T. Hankemeier is a shareholder in Mimetas B.V. All other authors declare no competing interests.

DATA AVAILABILITY STATEMENT

The data that support the findings of this study are available in the Materials and Methods, Results, and Supplementary Material of this article. Additional data will be provided upon request.

ORCID

Kanchana Pandian https://orcid.org/0000-0002-2825-637X
Luojiao Huang https://orcid.org/0000-0001-5825-5127
Abidemi Junaid https://orcid.org/0000-0001-8562-7942
Amy Harms https://orcid.org/0000-0002-2931-4295
Anton Jan van Zonneveld https://orcid.org/0000-0002-1676-7738
Thomas Hankemeier https://orcid.org/0000-0001-7871-2073

REFERENCES

1. Hickok JR, Vasudevan D, Jablonski K, Thomas DD. Oxygen dependence of nitric oxide-mediated signaling. *Redox Biol.* 2013;1(1):203-209. doi:10.1016/j.redox.2012.11.002

2. Bauer PM, Fulton D, Boo YC, et al. Compensatory phosphorylation and protein-protein interactions revealed by loss of function and gain of function mutants of multiple serine phosphorylation sites in endothelial nitric-oxide synthase*. *J Biol Chem.* 2003;278(17):14841-14849. doi:10.1074/jbc.M211926200

3. Archer SL, Huang JM, Hampl V, Nelson DP, Shultz PJ, Weir EK. Nitric oxide and cGMP cause vasorelaxation by activation of a charybdotoxin-sensitive K channel by cGMP-dependent protein kinase. *Proc Natl Acad Sci USA.* 1994;91(16):7583-7587. doi:10.1073/pnas.91.16.7583

4. Russo G, Leopold JA, Loscalzo J. Vasoactive substances: nitric oxide and endothelial dysfunction in atherosclerosis. *Vasc Pharmacol.* 2002;38(5):259-269. doi:10.1016/s1537-1891(02)00250-1

5. Murad F. Discovery of some of the biological effects of nitric oxide and its role in cell signaling. *Biosci Rep.* 2004;24(4–5):452-474. doi:10.1007/s10540-005-2741-8

6. Kingwell BA. Nitric oxide as a metabolic regulator during exercise: effects of training in health and disease. *Clin Exp Pharmacol Physiol.* 2000;27(4):239-250. doi:10.1046/j.1440-1681.2000.03232.x

7. Trochu JN, Bouhour JB, Kaley G, Hintze TH. Role of endothelium-derived nitric oxide in the regulation of cardiac oxygen metabolism. *Circ Res.* 2000;87(12):1108-1117. doi:10.1161/01.RES.87.12.1108

8. Pechánová O, Varga ZV, Cebová M, Giricz Z, Pacher P, Ferdinandy P. Cardiac NO signalling in the metabolic syndrome. *Br J Pharmacol.* 2015;172(6):1415-1433. doi:10.1111/bph.12960

9. Feng Q, Hedner T. Endothelium-derived relaxing factor (EDRF) and nitric oxide (NO). II. Physiology, pharmacology and pathophysiological implications. *Clin Physiol.* 1990;10(6):503-526. doi:10.1111/j.1475-097x.1990.tb00443.x

10. Flammer AJ, Lüscher TF. Human endothelial dysfunction: EDRFs. *Pflugers Arch.* 2010;459(6):1005-1013. doi:10.1007/s00424-010-0822-4

11. Bevers LM, Braam B, Post JA, et al. Tetrahydrobiopterin, but not L-arginine, decreases NO synthase uncoupling in cells expressing high levels of endothelial NO synthase. *Hypertension.* 2006;47(1):87-94. doi:10.1161/01.HYP.0000196735.85398.0e

12. Chen CA, Wang TY, Varadharaj S, et al. S-glutathionylation uncouples eNOS and regulates its cellular and vascular function. *Nature.* 2010;468(7327):1115-1118. doi:10.1038/nature09599

13. De Pascali F, Hemann C, Samons K, Chen CA, Zweier JL. Hypoxia and reoxygenation induce endothelial nitric oxide synthase uncoupling in endothelial cells through tetrahydrobiopterin depletion and S-glutathionylation. *Biochemistry.* 2014;53(22):3679-3688. doi:10.1021/bi500076r

14. McNeill E, Channon KM. The role of tetrahydrobiopterin in inflammation and cardiovascular disease. *Thromb Haemost.* 2012;108(5):832-839. doi:10.1160/TH12-06-0424

15. Wu F, Szczepaniak WS, Shiva S, et al. Nox2-dependent glutathionylation of endothelial NOS leads to uncoupled superoxide production and endothelial barrier dysfunction in acute lung injury. *Am J Physiol Lung Cell Mol Physiol.* 2014;307(12):L987-L997. doi:10.1152/ajplung.00063.2014

16. Yang YM, Huang A, Kaley G, Sun D. eNOS uncoupling and endothelial dysfunction in aged vessels. *Am J Physiol Heart Circ Physiol.* 2009;297(5):H1829-H1836. doi:10.1152/ajpheart.00230.2009

17. Cabral PD, Hong NJ, Garvin JL. Shear stress increases nitric oxide production in thick ascending limbs. *Am J Physiol Renal Physiol.* 2010;299(5):F1185-F1192. doi:10.1152/ajprenal.00112.2010

18. Tanaka K, Joshi D, Timalsina S, Schwartz MA. Early events in endothelial flow sensing. *Cytoskeleton.* 2021;78(6):217-231. doi:10.1002/cm.21652

19. Corson MA, James NL, Latta SE, Nerem RM, Berk BC, Harrison DG. Phosphorylation of endothelial nitric oxide synthase in response to fluid shear stress. *Circ Res.* 1996;79(5):984-991. doi:10.1161/01.RES.79.5.984

20. Fleming I, Fisslthaler B, Dixit M, Busse R. Role of PECAM-1 in the shear-stress-induced activation of Akt and the endothelial

nitric oxide synthase (eNOS) in endothelial cells. *J Cell Sci*. 2005;118(18):4103-4111. doi:10.1242/jcs.02541

21. Nagel T, Resnick N, Dewey CF, Gimbrone MA. Vascular endothelial cells respond to spatial gradients in fluid shear stress by enhanced activation of transcription factors. *Arterioscler Thromb Vasc Biol*. 1999;19(8):1825-1834. doi:10.1161/01.ATV.19.8.1825

22. Tovar-Lopez F, Thurgood P, Gilliam C, et al. A microfluidic system for studying the effects of disturbed flow on endothelial cells. *Front Bioeng Biotechnol*. 2019;7:1-7. doi:10.3389/fbioe.2019.00081

23. Williams D, Mahmoud MS, Liu R, et al. Stable flow-induced expression of KLK10 inhibits endothelial inflammation and atherosclerosis. *bioRxiv*. 2021. doi:10.1101/2021.08.10.455857

24. Barak OF, Mladinov S, Hoiland RL, et al. Disturbed blood flow worsens endothelial dysfunction in moderate-severe chronic obstructive pulmonary disease. *Sci Rep*. 2017;7(1):16929. doi:10.1038/s41598-017-17249-6

25. Junaid A, Schoeman J, Yang W, et al. Metabolic response of blood vessels to TNFα. *elife*. 2020;9:e54754. doi:10.7554/eLife.54754

26. Cabrera AP, Stoddard J, Santiago Tierno I, et al. Increased cell stiffness contributes to complement-mediated injury of choroidal endothelial cells in a monkey model of early age-related macular degeneration. *J Pathol*. 2022;257(3):314-326. doi:10.1002/path.5892

27. Circulation Research. Between Rho(k) and a hard place. doi:10.1161/CIRCRESAHA.116.305720

28. Schaefer A, Hordijk PL. Cell-stiffness-induced mechanosignaling – a key driver of leukocyte transendothelial migration. *J Cell Sci*. 2015;128(13):2221-2230. doi:10.1242/jcs.163055

29. van Duinen V, van den Heuvel A, Trietsch SJ, et al. 96 perfusable blood vessels to study vascular permeability in vitro. *Sci Rep*. 2017;7(1):18071. doi:10.1038/s41598-017-14716-y

30. Taylor DR, Pijnenburg MW, Smith AD, Jongste JCD. Exhaled nitric oxide measurements: clinical application and interpretation. *Thorax*. 2006;61(9):817-827. doi:10.1136/thx.2005.056093

31. Sandrini A, Taylor DR, Thomas PS, Yates DH. Fractional exhaled nitric oxide in asthma: an update. *Respirology*. 2010;15(1):57-70. doi:10.1111/j.1440-1843.2009.01616.x

32. Vidanapathirana AK, Pullen BJ, Zhang R, et al. A novel ruthenium-based molecular sensor to detect endothelial nitric oxide. *Sci Rep*. 2019;9(1):1720. doi:10.1038/s41598-019-39123-3

33. Hunter RA, Schoenfisch MH. S-Nitrosothiol analysis via photolysis and amperometric nitric oxide detection in a microfluidic device. *Anal Chem*. 2015;87(6):3171-3176. doi:10.1021/ac503220z

34. Moon J, Ha Y, Kim M, Sim J, Lee Y, Suh M. Dual electrochemical microsensor for real-time simultaneous monitoring of nitric oxide and potassium ion changes in a rat brain during spontaneous neocortical epileptic seizure. *Anal Chem*. 2016;88(18):8942-8948. doi:10.1021/acs.analchem.6b02396

35. Chokkathukalam A, Kim DH, Barrett MP, Breitling R, Creek DJ. Stable isotope-labeling studies in metabolomics: new insights into structure and dynamics of metabolic networks. *Bioanalysis*. 2014;6(4):511-524. doi:10.4155/bio.13.348

36. Paul Lee WN, Wahjudi PN, Xu J, Go VL. Tracer-based metabolomics: concepts and practices. *Clin Biochem*. 2010;43(16–17):1269-1277. doi:10.1016/j.clinbiochem.2010.07.027

37. Siervo M, Stephan BCM, Feelisch M, Bluck LJC. Measurement of in vivo nitric oxide synthesis in humans using stable isotopic methods: a systematic review. *Free Radic Biol Med*. 2011;51(4):795-804. doi:10.1016/j.freeradbiomed.2011.05.032

38. Gambardella J, Khondkar W, Morelli MB, Wang X, Santulli G, Trimarco V. Arginine and endothelial function. *Biomedicine*. 2020;8(8):277. doi:10.3390/biomedicines8080277

39. Shatanawi A, Momani MS, Al-Aqtash R, Hamdan MH, Gharaibeh MN. L-citrulline supplementation increases plasma nitric oxide levels and reduces arginase activity in patients with type 2 diabetes. *Front Pharmacol*. 2020;11:1-7. doi:10.3389/fphar.2020.584669

40. Figueroa A, Jaime SJ, Morita M, Gonzales JU, Moinard C. L-citrulline supports vascular and muscular benefits of exercise training in older adults. *Exerc Sport Sci Rev*. 2020;48(3):133-139. doi:10.1249/JES.0000000000000223

41. Kucharzewska P, Welch JE, Svensson KJ, Belting M. Ornithine decarboxylase and extracellular polyamines regulate microvascular sprouting and actin cytoskeleton dynamics in endothelial cells. *Exp Cell Res*. 2010;316(16):2683-2691. doi:10.1016/j.yexcr.2010.05.033

42. Shin BS, Fung HL, Upadhyay M, Shin S. Estimation of nitric oxide synthase activity via LC-MS/MS determination of 15N3-citrulline in biological samples. *Rapid Commun Mass Spectrom*. 2015;29(5):447-455. doi:10.1002/rcm.7124

43. Junaid A. *Microengineered Human Blood Vessels for Next Generation Drug Discovery*. Leiden University Dissertation; 2020. Accessed February 8, 2024. https://hdl.handle.net/1887/138650

44. Noga MJ, Dane A, Shi S, et al. Metabolomics of cerebrospinal fluid reveals changes in the central nervous system metabolism in a rat model of multiple sclerosis. *Metabolomics*. 2012;8(2):253-263. doi:10.1007/s11306-011-0306-3

45. Feliers D, Chen X, Akis N, Choudhury GG, Madaio M, Kasinath BS. VEGF regulation of endothelial nitric oxide synthase in glomerular endothelial cells. *Kidney Int*. 2005;68(4):1648-1659. doi:10.1111/j.1523-1755.2005.00575.x

46. Rees DD, Palmer RM, Schulz R, Hodson HF, Moncada S. Characterization of three inhibitors of endothelial nitric oxide synthase in vitro and in vivo. *Br J Pharmacol*. 1990;101(3):746-752. doi:10.1111/j.1476-5381.1990.tb14151.x

47. da SFC, de ABJ, Cordeiro CS, et al. Endothelial dysfunction due to the inhibition of the synthesis of nitric oxide: proposal and characterization of an in vitro cellular model. *Front Physiol*. 2022;13:1-13. doi:10.3389/fphys.2022.978378

48. Caldwell RB, Toque HA, Narayanan SP, Caldwell RW. Arginase: an old enzyme with new tricks. *Trends Pharmacol Sci*. 2015;36(6):395-405. doi:10.1016/j.tips.2015.03.006

49. Grover TR, Zenge JP, Parker TA, Abman SH. Vascular endothelial growth factor causes pulmonary vasodilation through activation of the phosphatidylinositol-3-kinase-nitric oxide pathway in the late-gestation ovine fetus. *Pediatr Res*. 2002;52(6):907-912. doi:10.1203/00006450-200212000-00016

50. Pandey AK, Singhi EK, Arroyo JP, et al. Mechanisms of VEGF (vascular endothelial growth factor) inhibitor-associated hypertension and vascular disease. *Hypertension*. 2018;71(2):e1-e8. doi:10.1161/HYPERTENSIONAHA.117.10271

51. Cazzaniga A, Locatelli L, Castiglioni S, Maier J. The contribution of EDF1 to PPARγ transcriptional activation in VEGF-treated human endothelial cells. *Int J Mol Sci*. 2018;19(7):1830. doi:10.3390/ijms19071830

52. Gélinas DS, Bernatchez PN, Rollin S, Bazan NG, Sirois MG. Immediate and delayed VEGF-mediated NO synthesis in endothelial cells: role of PI3K, PKC and PLC pathways. *Br J Pharmacol*. 2002;137(7):1021-1030. doi:10.1038/sj.bjp.0704956

53. Colleluori DM, Ash DE. Classical and slow-binding inhibitors of human type II arginase. *Biochemistry*. 2001;40(31):9356-9362. doi:10.1021/bi010783g

54. Hecker M, Sessa WC, Harris HJ, Änggård EE, Vane JR. The metabolism of L-arginine and its significance for the biosynthesis of endothelium-derived relaxing factor: cultured endothelial cells recycle L- citrulline to L-arginine. *Proc Natl Acad Sci USA*. 1990;87(21):8612-8616.

55. Tsuboi T, Maeda M, Hayashi T. Administration of L-arginine plus L-citrulline or L-citrulline alone successfully retarded endothelial senescence. *PLoS One*. 2018;13(2):e0192252. doi:10.1371/journal.pone.0192252

56. Molnos S, Wahl S, Haid M, et al. Metabolite ratios as potential biomarkers for type 2 diabetes: a DIRECT study. *Diabetologia*. 2018;61(1):117-129. doi:10.1007/s00125-017-4436-7

57. Lin YJ, Hsu CN, Lo MH, Huang CF, Chien SJ, Tain YL. High citrulline-to-arginine ratio associated with blood pressure abnormalities in children with early chronic kidney disease. *Circ J*. 2013;77(1):181-187. doi:10.1253/circj.cj-12-0602

58. Lin IC, Hsu CN, Lo MH, Chien SJ, Tain YL. Low urinary citrulline/arginine ratio associated with blood pressure abnormalities and arterial stiffness in childhood chronic kidney disease. *J Am Soc Hypertens*. 2016;10(2):115-123. doi:10.1016/j.jash.2015.11.008

59. Shatanawi A, Momani MS. Arginase inhibition improves vascular function and restores NO production in diabetic conditions. *FASEB J*. 2018;32(S1):569.7. doi:10.1096/fasebj.2018.32.1_supplement.569.7

60. Neul JH, Kang H, Lee A, et al. Endothelial miR-26a regulates VEGF-Nogo-B receptor-mediated angiogenesis. *BMB Rep*. 2017;50(7):384-389. doi:10.5483/BMBRep.2017.50.7.085

61. Ryoo S, Gupta G, Benjo A, et al. Endothelial arginase II. *Circ Res*. 2008;102(8):923-932. doi:10.1161/CIRCRESAHA.107.169573

62. Cooke JP, Rossitch E, Andon NA, Loscalzo J, Dzau VJ. Flow activates an endothelial potassium channel to release an endogenous nitrovasodilator. *J Clin Invest*. 1991;88(5):1663-1671. doi:10.1172/JCI115481

63. Zhou J, Li YS, Chien S. Shear stress-initiated signaling and its regulation of endothelial function. *Arterioscler Thromb Vasc Biol*. 2014;34(10):2191-2198. doi:10.1161/ATVBAHA.114.303422

64. Wang N, Miao H, Li YS, et al. Shear stress regulation of Krüppel-like factor 2 expression is flow pattern-specific. *Biochem Biophys Res Commun*. 2006;341(4):1244-1251. doi:10.1016/j.bbrc.2006.01.089

65. Turpaev KT. Transcription factor KLF2 and its role in the regulation of inflammatory processes. *Biochem Mosc*. 2020;85(1):54-68.

66. Vaisman BL, Andrews KL, Khong SML, et al. Selective endothelial overexpression of arginase II induces endothelial dysfunction and hypertension and enhances atherosclerosis in mice. *PLoS One*. 2012;7(7):e39487. doi:10.1371/journal.pone.0039487

67. Kövamees O, Shemyakin A, Pernow J. Amino acid metabolism reflecting arginase activity is increased in patients with type 2 diabetes and associated with endothelial dysfunction. *Diab Vasc Dis Res*. 2016;13(5):354-360. doi:10.1177/1479164116643916

68. Decker B, Pumiglia K. mTORc1 activity is necessary and sufficient for phosphorylation of eNOSS1177. *Physiol Rep*. 2018;6(12):e13733. doi:10.14814/phy2.13733

69. Mammedova JT, Sokolov AV, Freidlin IS, Starikova EA. The mechanisms of L-arginine metabolism disorder in endothelial cells. *Biochemistry (Mosc)*. 2021;86(2):146-155. doi:10.1134/S0006297921020036

70. Noris M, Morigi M, Donadelli R, et al. Nitric oxide synthesis by cultured endothelial cells is modulated by flow conditions. *Circ Res*. 1995;76(4):536-543. doi:10.1161/01.RES.76.4.536

SUPPORTING INFORMATION

Additional supporting information can be found online in the Supporting Information section at the end of this article.